

UC Berkeley

UC Berkeley Previously Published Works

Title

Complex Roles of PsbS and Xanthophylls in the Regulation of Nonphotochemical Quenching in *Arabidopsis thaliana* under Fluctuating Light

Permalink

<https://escholarship.org/uc/item/4fn949mc>

Journal

The Journal of Physical Chemistry B, 124(46)

ISSN

1520-6106

Authors

Steen, Collin J
Morris, Jonathan M
Short, Audrey H
et al.

Publication Date

2020-11-19

DOI

10.1021/acs.jpcc.0c06265

Peer reviewed

Complex Roles of PsbS and Xanthophylls in the Regulation of Nonphotochemical Quenching in *Arabidopsis thaliana* under Fluctuating Light

Collin J. Steen, Jonathan M. Morris, Audrey H. Short, Krishna K. Niyogi, and Graham R. Fleming*

Cite This: *J. Phys. Chem. B* 2020, 124, 10311–10325

Read Online

ACCESS |

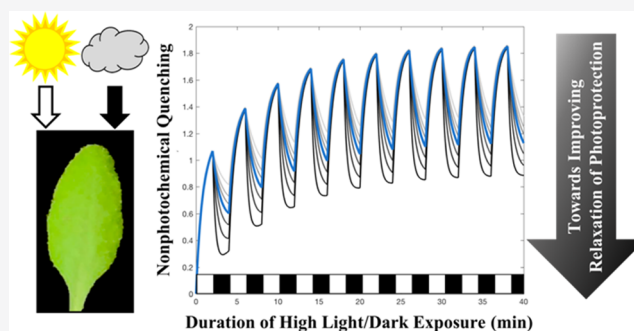
Metrics & More

Article Recommendations

Supporting Information

ABSTRACT: Protection of photosystem II against damage from excess light by nonphotochemical quenching (NPQ) includes responses on a wide range of timescales. The onset of the various phases of NPQ overlap in time making it difficult to discern if they influence each other or involve different photophysical mechanisms. To unravel the complex relationship of the known actors in NPQ, we perform fluorescence lifetime snapshot measurements throughout multiple cycles of alternating 2 min periods of high light and darkness. By comparing the data with an empirically based mathematical model that describes both fast and slow quenching responses, we suggest that the rapidly reversible quenching response depends on the state of the slower response.

By studying a series of *Arabidopsis thaliana* mutants, we find that removing zeaxanthin (Zea) or enhancing PsbS concentration, for example, influences the amplitudes of the slow quenching induction and recovery, but not the timescales. The plants' immediate response to high light appears independent of the illumination history, while PsbS and Zea have distinct roles in both quenching and recovery. We further identify two parameters in our model that predominately influence the recovery amplitude and propose that our approach may prove useful for screening new mutants or overexpressors with enhanced biomass yields under field conditions.



INTRODUCTION

The initial step of photosynthesis requires absorption of light to drive charge separation via photochemistry.¹ However, fluctuating sunlight can transiently exceed the capacity of photosynthetic organisms to use the absorbed energy for productive charge separation. To avoid damage to the photosynthetic apparatus, photosynthetic organisms regulate photoprotective processes in response to light conditions, ensuring that excess energy is dissipated safely.² Recent work has shown that increasing photosynthetic organisms' ability to rapidly match the level of photoprotection to incident light conditions can improve crop yields.^{3,4} Nonetheless, the individual contributions of the various biochemical actors are still under debate, especially under natural light conditions.

When light absorption outpaces charge separation, photosystem II (PSII) experiences longer-lived excitation kinetics^{2,5} and is more susceptible to damage than photosystem I.^{2,6–8} The suite of photoprotective mechanisms that protect PSII by dissipating excess excitation—referred to collectively as nonphotochemical quenching (NPQ), the reduction in the observed chlorophyll *a* (Chl *a*) fluorescence by mechanisms other than photochemistry^{9–11}—have been the subject of intense study.

The contributions to overall NPQ are often separated into components, including (but not limited to) qE ^{12–17} (rapidly

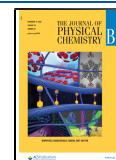
reversible phase), qZ ^{18–21} (dependent on zeaxanthin (Zea)), and qI ^{22–25} (associated with photoinhibition). More recently, a slowly reversible component called qH (which is induced by a combination of high light (HL) and low temperature) has been added.²⁶ However, many of the NPQ components overlap in time and it is not clear if they involve the same underlying photophysical dissipation mechanism(s) controlled by different kinetic regulatory processes or utilize differing dissipation mechanisms. To unravel the complex relationships of the known actors in NPQ, rather than measuring the response of leaves over a single light–dark cycle, we employ multiple cycles of short (2 min) periods of high light (HL) alternating with dark periods of the same duration.

Rapidly alternating HL and dark periods over a series of 10 cycles allows us to measure how the rapid response evolves as the slow responses simultaneously move toward their steady-state behavior. This periodic illumination sequence is also more representative of the fluctuating light exposure patterns

Received: July 8, 2020

Revised: October 7, 2020

Published: November 9, 2020



that plants experience in nature.^{4,27–30} By combining these data with a mathematical model that incorporates both fast and slow responses, but which is agnostic as to the specific molecular mechanisms underlying the components, we demonstrate that the rapidly reversible response depends on the slower response.

Here, time-correlated single photon counting (TCSPC) measurements of the fluorescence lifetime are performed on whole *Arabidopsis thaliana* leaves under exposure to periodic actinic light. As discussed elsewhere,³¹ directly measuring the fluorescence lifetimes in snapshots enables us to focus only on processes that quench chlorophyll excitations. As opposed to fluorescence yields, fluorescence lifetimes are not influenced by processes that reduce the fluorescence quantum yield but do not result in quenching of chlorophyll excitation,^{32,33} such as enhanced light scattering, chloroplast movement,³⁴ or chromophore bleaching.

To disentangle how the various known biochemical actors influence the timescales and amplitudes of the quenching response, we utilized a range of mutants for comparison to wild type (WT, Col-0 ecotype; see Table 1 for a summary of all

Table 1. *A. thaliana* Genotypes Investigated in This Study^a

Abbreviation	Phenotype	Reference
WT	wild type	
L17	overexpresses PsbS	37
sz11	minimal [Zea], increased [Lut]	45, 50
npq4	lacks PsbS function	35
npq1	no VDE activity	48, 49

^aThe color of each genotype matches those used throughout the manuscript.

genotypes). As the involvement of the pH-sensing protein PsbS in qE is well established,^{35,36} we selected a PsbS-deficient mutant, *npq4*, and a PsbS-overexpressing mutant, *L17*.³⁷ Similarly, low lumen pH activates the enzyme violaxanthin de-epoxidase (VDE) which converts violaxanthin via antheraxanthin to zeaxanthin (Zea) in the HL-dependent half of the VAZ cycle.^{2,9,10,38} There has been extensive discussion in the literature concerning the role(s) of Zea^{39–43} and another de-epoxidized xanthophyll—lutein (Lut)^{44–47}—in the dissipation mechanism underlying NPQ. Accordingly, we utilized the mutant *npq1*, which lacks VDE and is unable to generate Zea,^{48,49} and the *sz11* mutant, which does not accumulate Zea but possesses increased levels of lutein.^{45,50}

By considering these various mutants in the context of our model, we discuss the molecular species and identify specific model parameters controlling the extent of recovery from maximum quenching. We propose that determination of these parameters could provide a rapid method for selecting new mutants and overexpressors with enhanced recovery amplitudes for field trials aimed at increasing biomass yields.

METHODS AND DATA ANALYSIS

Plant Genotypes and Growth Conditions. Five *A. thaliana* genetic lines were selected for a comparison of the effects of both PsbS and xanthophylls (Zea and Lut) in rapid and moderate-to-long timescale quenching dynamics usually classified as qE, qZ, or qI. The specific genotypes studied are summarized in Table 1. Plants were germinated on MS plates, transplanted to pots after 2 weeks, and grown in growth chambers under 110 $\mu\text{mol photons m}^{-2} \text{s}^{-1}$ on a 10-h day and

14-h night cycle at 23 °C. All plants were between 5 and 8 weeks of age at the time of experiments.

TCSPC Measurements and Exponential Fitting. Chlorophyll fluorescence lifetime snapshot measurements of whole leaves of *A. thaliana* were collected via time-correlated single photon counting (TCSPC) to measure changes in the fluorescence lifetimes (picoseconds to nanoseconds) of chlorophyll *a* (Chl *a*) in PSII in response to high-light exposure (seconds to minutes). TCSPC fluorescence lifetime measurements are less sensitive to changes in absorbance, due to e.g., chloroplast avoidance, than traditional yield measurements,³¹ allowing lengthier actinic light exposure patterns to be studied.

After an hour of initial dark acclimation, leaves were removed from the plant and placed in a custom-built sample holder. A 532 nm Coherent Verdi G10 diode laser pumped an ultrafast Ti:sapphire Coherent Mira 900f oscillator with a center wavelength of 840 nm and full width at half-maximum (FWHM) of approximately 9 nm. The 840 nm output pulses from the Mira were then frequency doubled to 420 nm using a β -barium borate crystal to excite the Soret band of Chl *a*. The beam was split, with a portion directed to a sync photodiode providing a reference for TCSPC measurements and the remainder directed to the sample. The portion of the beam that reached the sample was incident on the leaf at a $\sim 70^\circ$ angle to the adaxial side of the leaf. The average power of the laser at the sample was 1.75 mW, saturating reaction centers.⁵¹ Fluorescence was collected through a monochromator (HORIBA Jobin-Yvon; H-20) set to transmit 680 ± 8 nm placed before a microchannel plate (MCP)-photomultiplier tube (PMT) detector (Hamamatsu R3809U MCP-PMT) to selectively observe fluorescence from the Q_y band of Chl *a* in PSII. The detector was cooled to -30 °C and the gain was set to 94% yielding an instrument response function with a FWHM of 36–38 ps. Data were acquired using a Becker & Hickl SPC-850 data acquisition card combined with a sequence of trigger and shutter operations executed with LabView. The actinic light source was a Leica KL1500 LCD with a peak intensity of 648 nm and FWHM of 220 nm. TCSPC snapshots were collected at 30 s intervals over 10 4 min cycles consisting of 2 min of high light (700 $\mu\text{mol photons m}^{-2} \text{s}^{-1}$ actinic white light) and 2 min of darkness. Fluorescence decays were collected for each of the 0.2 s steps during the 1 s snapshot measurement and fit to biexponential functions using reconvolution fitting with the measured instrument response function. The amplitude-weighted average lifetime for each decay was calculated, and the step with the longest lifetime was chosen as the step with the reaction centers closed to saturation, as described in the previous work.^{52,53}

Data and Error Analysis. High snapshot time resolution is required to resolve the timescale of the rapid induction and relaxation of quenching upon transitions between darkness and high light. Measurements at 30 s snapshot resolution were collected for two “time offsets” describing the initial timepoint: one starting at 0 s (resulting in measurements at 0, 30, 60 s, and so on) and another at 15 s (resulting in measurements at 15, 45, 75 s, and so on). To achieve a final data set with 15 s snapshot resolution, pairwise permutations of 0 and 15 s leaf samples were combined and a first-order Butterworth filter with a critical frequency of 15 s^{-1} was applied to remove high-frequency oscillations due to leaf-to-leaf variability. The resulting filtered traces were averaged at each timepoint to

obtain fluorescence lifetime snapshot traces and uncertainty was estimated as the standard error, where the number of independent samples was the number of filtered, pairwise permutations for each genotype. For example, three independent leaves measured using both the 0 and 15 s sequences yields nine possible pairwise permutations.

To quantify quenching, NPQ_τ values were calculated from the mean snapshot lifetime traces, as previously described.^{31,42,43} The formula for NPQ_τ is analogous to the traditional NPQ parameter^{1,48,54} ($\text{NPQ} = (F_m - F_m')/F_m'$). The error in NPQ_τ was again estimated as the standard error. To quantify the interperiod behavior, upper and lower envelope traces were obtained by selecting the NPQ_τ values at the light-to-dark transitions (maximum quenching) and dark-to-light transitions (maximum recovery) and these data points were fit to an exponential function of the form $a e^{-t/\tau} + c$, where a was negative. To quantify the intraperiod behavior at steady state, the data from the penultimate (ninth) HL and dark periods were fit to an exponential function of the form $a e^{-t/\tau} + c$, where a was negative.

All data analysis and modeling was performed using MATLAB. In all cases, the model's differential equation (eq 1 in Box 1) was integrated over the duration of the experiment

Box 1. Equations for Model.

$$\frac{dq_{\text{active}}}{dt} = -[k_1(t) + k_2(t)]q_{\text{active}} + k_2(t) \quad (1)$$

Structure of the rate constants:

$$k_1(t) = k_1^{\text{rapid}}(t) + k_1^{\text{quenching envelope}} + k_1^{\text{recovery envelope}} \quad (2)$$

$$k_2(t) = k_2^{\text{rapid}}(t) + k_2^{\text{quenching envelope}} + k_2^{\text{recovery envelope}} \quad (3)$$

Structure of the intra-period rate constants:

$$k_1^{\text{rapid}}(t) = \begin{cases} \frac{1}{\tau_{\text{rapid}}^{\text{light}}} (1 - q_{\text{max}}(t)), & \text{light} \\ \frac{1}{\tau_{\text{rapid}}^{\text{dark}}} (1 - q_{\text{rec}}(t)), & \text{dark} \end{cases} \quad (4)$$

$$k_2^{\text{rapid}}(t) = \begin{cases} \frac{1}{\tau_{\text{rapid}}^{\text{light}}} q_{\text{max}}(t), & \text{light} \\ \frac{1}{\tau_{\text{rapid}}^{\text{dark}}} q_{\text{rec}}(t), & \text{dark} \end{cases} \quad (5)$$

(where $q_{\text{max}}(t) = a_{\text{max}} e^{-t/\tau_{\text{max}}} + c_{\text{max}}$ and $q_{\text{rec}}(t) = a_{\text{rec}} e^{-t/\tau_{\text{rec}}} + c_{\text{rec}}$)

Structure of the time-independent inter-period rate constants:

$$k_1^{\text{quenching envelope}} = \frac{1}{\tau_{\text{max}}^{\text{inter}}} (1 - c_{\text{max}}) \quad (6)$$

$$k_2^{\text{quenching envelope}} = \frac{1}{\tau_{\text{max}}^{\text{inter}}} c_{\text{max}} \quad (7)$$

$$k_1^{\text{recovery envelope}} = \frac{1}{\tau_{\text{rec}}^{\text{inter}}} (1 - c_{\text{rec}}) \quad (8)$$

$$k_2^{\text{recovery envelope}} = \frac{1}{\tau_{\text{rec}}^{\text{inter}}} c_{\text{rec}} \quad (9)$$

*Terms in green come from fits to rapid intra-period dynamics (penultimate period #9).

*Terms in blue come from fits to slowly-varying inter-period envelopes.

*Terms in red contain both fast and slow timescales.

(0–40 min) in steps of 0.005 min using the fourth order Runge–Kutta (RK4) method. The structure of the model and the necessary equations are described extensively in the main text and the individual model parameters are also described in the Supporting Information (SI) section titled “Discussion of Model Parameters”.

RESULTS AND EMPIRICAL FITTING

Fluorescence lifetime snapshot measurements were collected at 15 s resolution on intact leaves from the five *A. thaliana* strains

listed in Table 1. Detailed descriptions of the fluorescence lifetime data accumulation, combination of different time offsets, and filtering to eliminate the leaf-to-leaf variability within a single strain are given in the Supporting Information (see “Analysis of Fluorescence Lifetime Snapshot Traces”). Fluorescence lifetime determinations of NPQ have a number of advantages over the more standard pulse amplitude modulated (PAM) fluorescence method,³¹ as discussed in the Introduction. To convert the measured average fluorescence decay lifetimes to a unitless form similar to the NPQ value obtained from PAM measurements, we define $\text{NPQ}_\tau(t) = \frac{\tau_{\text{dark}}(t=0) - \tau_{\text{light}}(t)}{\tau_{\text{light}}(t)}$,^{31,42,54,55} where τ is the amplitude-weighted average lifetime from a biexponential fit. NPQ_τ also enables the direct comparison of different mutants that have slightly different dark-state lifetimes.

Figure 1 shows the values of NPQ_τ for each strain over 10 light–dark cycles. During high light (HL, 700 $\mu\text{mol photons}$

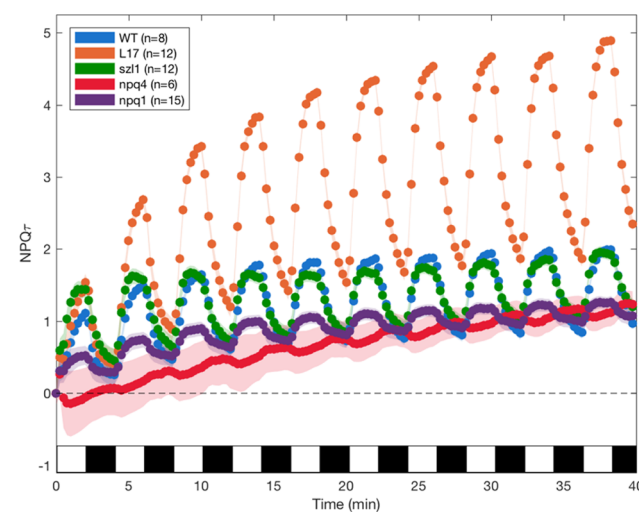


Figure 1. Comparison of NPQ_τ traces for each strain: WT (blue), L17 (orange), *szl1* (green), *npq4* (red), and *npq1* (purple). The PsbS-containing lines (WT, L17, *szl1*, and *npq1*) show oscillatory quenching induction and relaxation within each period. The PsbS-deficient mutant *npq4* does not show the strong oscillatory behavior and the Zea-deficient mutant *npq1* shows a dampened oscillatory behavior. Data are presented as the mean NPQ_τ value and the shaded regions represent the standard error. The number of independent leaf samples measured for each genotype is indicated in the legend.

$\text{m}^{-2} \text{s}^{-1}$), the quenching rapidly increases as the NPQ components turn on. During subsequent exposure to darkness, the quenching drops but the fluorescence lifetime does not fully return to the original dark-acclimated value (Figure S1). After a few HL–dark cycles, the lifetimes saturate at the maximum quenching value, followed a few cycles later by the saturation of the maximum recovery values. By the end of the 10 cycles, the dynamics have reached a periodic steady state, with only small variations between periods. In electronic circuits and in signal processing, the smooth curves that describe the time-dependent extrema are called “envelopes” and we will use this term.

All of the PsbS-containing lines (WT, *szl1*, L17, and *npq1*) show significant intraperiod responses, in agreement with previous conclusions about the role of PsbS in rapidly reversible quenching.^{3,11,35–37,41,42,52,56–59} Compared to WT (blue trace in Figure 1), L17 (PsbS overexpressor, orange

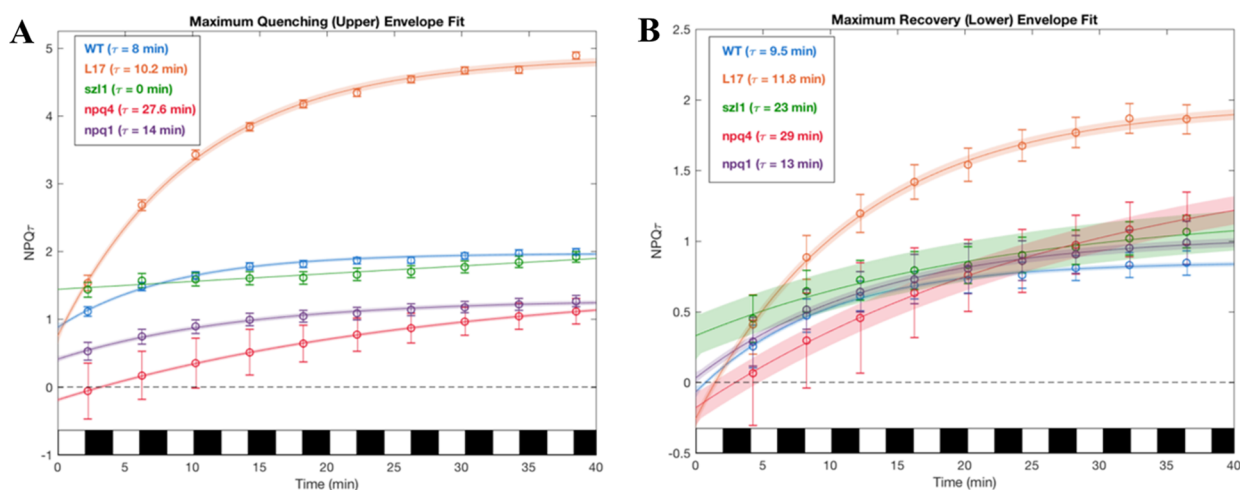


Figure 2. Slow interperiod dynamics of (A) maximum quenching envelope and (B) maximum recovery envelope. Open circles represent NPQ_τ trace values from Figure 1 selected at (A) the light-to-dark transition and (B) the dark-to-light transition and the error bars represent the standard error in NPQ_τ . The solid line represents the best fit to a single exponential decay and the shaded regions represent the standard error in the fit. The shaded error region is omitted for the *szl1* maximum quenching envelope due to the poor quality of the exponential fit (time constant significantly longer than the timescale of the experiment). The lifetimes (τ) obtained from fitting are listed in the legend and all fit values with errors are presented in Table 2.

trace) has an increased amplitude of rapidly reversible quenching and recovery, while *npq4* (inactive PsbS, red trace) almost entirely lacks rapidly reversible NPQ, both of which agree with previous observations.^{35,37,52,56} Under HL, VDE is active and Zea reaches near maximal accumulation in the first few periods, unable to return to antheraxanthin or violaxanthin in the short (2 min) dark relaxation time as revealed by previous high-performance liquid chromatography measurements.^{42,53} Therefore, in later periods the interperiod dynamics should be attributable to slowly reversible or irreversible quenching processes rather than changes in the carotenoid (i.e., Zea) pool or the presence/activity of PsbS.

The *npq1* mutant (lacks Zea, purple trace) still shows oscillations in NPQ, but the magnitude is greatly dampened relative to WT. Interestingly, *szl1* (excess Lut, green trace) displays quenching behavior qualitatively very similar to WT, despite its inability to accumulate detectable levels of Zea. These findings are consistent with previous suggestions that Lut is capable of quenching Chl excited states in the absence of Zea,^{44,45,60} though with a lower efficiency on a per-molecule basis.⁵³

Interperiod and Intraproduct Dynamics. Analysis of inter- and intraproduct dynamics allows for the separation of fast and slow quenching processes that depend on common biochemical regulators, such as the PsbS protein and various carotenoids. The quenching dynamics during the first few HL–dark cycles depend on the simultaneous action of fast and slow-timescale processes, making it difficult to interpret them separately. However, during the later HL–dark cycles, the observed intraproduct oscillations in NPQ_τ arise entirely from the magnitude and timescales of the rapidly reversible response because the moderate-to-long timescale responses have reached a steady state in terms of activation and relaxation. Thus, periodic illumination experiments allow for the rapid response that appears within single periods (intraproduct) to be distinguished from the moderate-timescale response that appears in period-to-period (interperiod) comparisons without requiring a direct comparison of different mutant lines. We note that the rapidly reversible response can

be considered as analogous to the traditional quenching component qE , while the moderate-timescale response can be considered as analogous to slower quenching components (e.g., qZ and qI). Framing the processes as temporal “responses” instead of biochemically regulated “components” allows us to separate the temporal overlap of the effects usually attributed to traditional components (qE , qZ , qI , etc.).

Figure 2 shows interperiod envelope traces of the maximum quenching NPQ_τ values and maximum recovery NPQ_τ values. To estimate the timescale and extent of the slowly varying interperiod behavior, both the upper and lower envelopes were fit to simple exponential decays. Although multiple biochemical processes occur with different timescales, such as the accumulation of Zea and longer-timescale protein and membrane structural reorganizations, only a single time constant was resolvable in the envelopes. Fit values are provided in Table 2.

The maximum induction timescale fit of zero for *szl1* suggests there are no interperiod quenching dynamics present at this temporal resolution; the level is constant or already at a “steady state”. In contrast, WT shows an 8 min timescale to achieve maximum quenching, similar to the timescale for the accumulation of Zea in various plants.^{42,53,55} There is excess Lut but no Zea accumulation in *szl1*, while WT possesses Lut and accumulates Zea in HL until a steady state is reached within a few periods. The differences between WT and the *szl1* mutant therefore suggest that the maximum quenching induction depends on both Zea and Lut accumulation. This could explain the faster initial induction of quenching in *szl1* compared to WT, as was previously observed for measurements during one or two HL–dark cycles.^{45,53} The even slower induction behavior for *npq1* (slower timescale of 14 min) further reinforces this dependence of NPQ on de-epoxidized carotenoids given that *npq1* entirely lacks Zea, but possesses Lut.^{45,48,49}

As mentioned above, the *npq4* mutant (deficient in PsbS) displays very little rapidly reversible quenching. However, it still shows a slow increase (timescale of 27.6 min) in the maximum quenching over successive periods. This moderate-

Table 2. Fit Values for Maximum Quenching and Recovery Envelopes^a: (A) Maximum Quenching Fit Values: $\text{NPQ}_\tau^{\text{max}}(t) = a e^{-t/\tau} + c$ and (B) Maximum Recovery Envelope Fit Values: $\text{NPQ}_\tau^{\text{min}}(t) = a e^{-t/\tau} + c$

(A)			
max quenching fits	<i>a</i>	τ (min)	<i>c</i>
WT	-1.09 ± 0.06	8 ± 1	1.97 ± 0.03
<i>L17</i>	-4.1 ± 0.1	10.2 ± 0.7	4.87 ± 0.06
<i>szl1</i>			
<i>npq4</i>	-1.73 ± 0.02	27.6 ± 0.8	1.54 ± 0.03
<i>npq1</i>	-0.88 ± 0.03	14 ± 2	1.29 ± 0.03
(B)			
max recovery fits	<i>a</i>	τ (min)	<i>c</i>
WT	-0.92 ± 0.04	9.5 ± 0.9	0.85 ± 0.02
<i>L17</i>	-2.23 ± 0.06	11.8 ± 0.8	1.97 ± 0.04
<i>szl1</i>	-0.9 ± 0.1	23 ± 8	1.2 ± 0.1
<i>npq4</i>	-1.88 ± 0.08	29 ± 3	1.7 ± 0.1
<i>npq1</i>	-1.01 ± 0.03	13 ± 1	1.04 ± 0.03

^aValues for exponential fits of the moderate-to-long timescale envelope dynamics for (A) the maximum quenching (upper) envelope fit obtained from selection of trace values at the light-to-dark transition and (B) the maximum recovery (lower) envelope fit obtained from selection of trace values at the dark-to-light transition. Note that no maximum quenching exponential lifetime component was observed for *szl1* within the timescale of the experiment; instead the maximum quenching envelope increased constantly. Fit values reported are the mean and error is the standard error of the fit reported to one significant digit. Parameters *a* and *c* are unitless values of NPQ_τ and τ is reported in minutes.

timescale quenching that occurs in the absence of PsbS appears to be distinct from the role that PsbS plays in photoinhibitory quenching (qI) under prolonged (>hour) HL illumination.^{27,37,56,61}

Beyond *szl1* and *npq4*, all other mutants exhibit similar timescales of maximum interperiod quenching and recovery as WT, although *npq1* is slightly slower with a 14 min induction timescale (Figure 2 and Table 2).

The rapid steady-state intraperiod dynamics are presented in Figure 3 with fit parameters listed in Table 3. These data come

Table 3. Rapidly Reversible Quenching Fit Values^a: (A) Induction Fit Values: $\text{NPQ}_\tau = a e^{-t/\tau} + c$ and (B) Relaxation Fit Values: $\text{NPQ}_\tau = a e^{-t/\tau} + c$

(A)			
induction fit values	<i>a</i>	τ (s)	<i>c</i>
WT	-1.3 ± 0.1	45 ± 11	2.1 ± 0.1
<i>L17</i>	-3.5 ± 0.4	46 ± 15	5.1 ± 0.4
<i>szl1</i>	-0.94 ± 0.07	36 ± 8	1.91 ± 0.06
<i>npq1</i>	-0.31 ± 0.03	32 ± 8	1.24 ± 0.02
(B)			
relaxation fit values	<i>a</i>	τ (s)	<i>c</i>
WT	1.6 ± 0.3	87 ± 28	0.4 ± 0.3
<i>L17</i>	3.5 ± 0.2	74 ± 11	1.2 ± 0.3
<i>szl1</i>	0.94 ± 0.07	63 ± 12	0.94 ± 0.08
<i>npq1</i>	0.23 ± 0.02	34 ± 7	1.00 ± 0.01
<i>npq4</i>	-0.14 ± 0.01	47 ± 6	1.18 ± 0.01

^aExponential fit values for quasi-periodic steady-state rapidly reversible (A) high-light induction and (B) dark recovery. Fit values reported are the mean and error is the standard error of the fit reported to one significant digit. Parameters *a* and *c* are unitless values of NPQ_τ and τ is reported in seconds.

from fits of the penultimate HL–dark cycle in Figure 1 and represent a quasi-periodic steady-state as the intraperiod timescales (time constants) were observed to remain unchanged after the third or fourth HL–dark cycle (Figure S2). Once the steady state has been reached, intraperiod HL quenching induction is consistently faster than the dark recovery with timescales of 30–50 and 60–90 s (Table 3), which may reflect the kinetics of ΔpH buildup and relaxation, respectively. Additionally, the intraperiod timescales are more or less the same for the different genotypes, suggesting that differences in the carotenoid composition or PsbS activity modulate the amplitude of rapidly reversible quenching but not the inherent timescales or kinetics. An exception is the

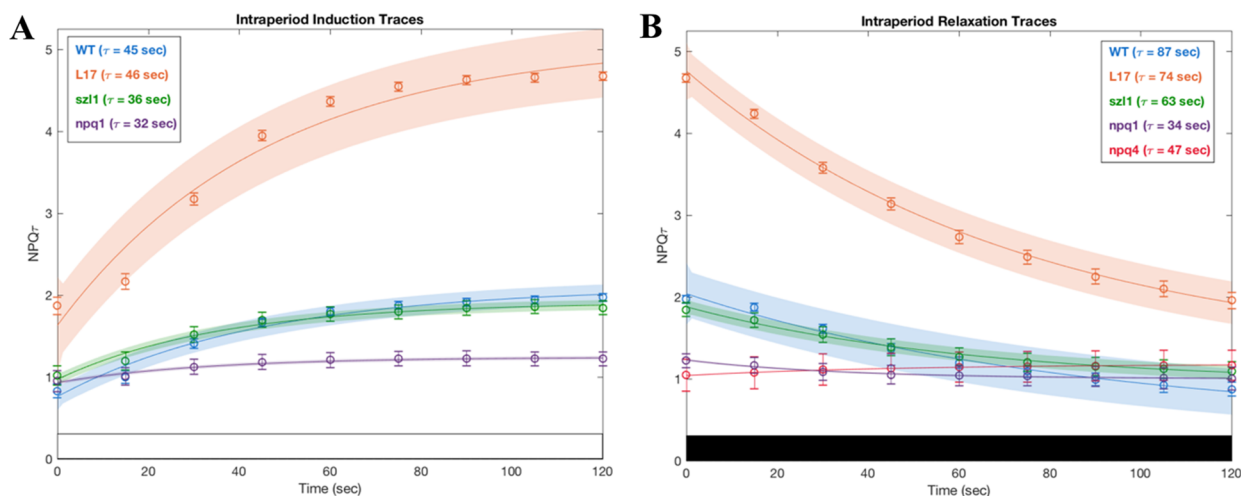
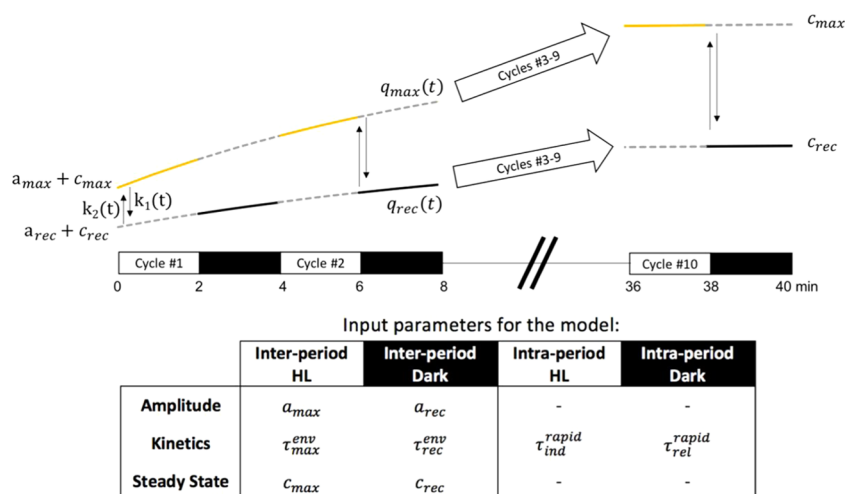


Figure 3. Rapidly reversible intraperiod dynamics of (A) high-light quenching induction and (B) dark relaxation. Data are presented as the NPQ_τ values (open circles) and error bars represent the standard error from the penultimate light and dark cycles presented in Figure 1 to ensure that a steady state has been reached. Solid lines represent the best fit to a single exponential decay and shaded regions indicate the standard error in the fit. The lifetimes (τ) obtained from fitting are listed in the legend and all fit values with errors are presented in Table 3.

Scheme 1. Diagrammatic Representation of the Mathematical Model Describing the Regulation of Quenching^a

^aQuenching is modeled by q^{active} whose trajectory is governed by two piecewise time-dependent rate constants, $k_1(t)$ and $k_2(t)$. The observed macroscopic quenching moves within the region between the maximum quenching ($q_{max}(t)$, yellow) and maximum recovery states ($q_{rec}(t)$, black), whose values are determined from empirical interperiod fit parameters (bottom table). The values for each of these eight parameters are determined from direct exponential fits to the experimental data for each genotype. The interperiod and intraperiod dynamics are fit to the same mathematical construction (a single exponential of the form $q = a e^{-t/\tau} + c$). Interperiod HL and dark values for a , τ^{env} , and c in addition to intraperiod HL and dark kinetics (τ^{rapid}) are the only inputs to the model.

intraperiod recovery in *npq1*, which is significantly faster at 34 s.

MATHEMATICAL MODEL OF MULTI-TIMESCALE REGULATORY PROCESSES

To draw additional conclusions regarding the various known molecular actors in NPQ and their timescales of quenching induction and recovery, we constructed a mathematical model that includes the simultaneous actions of rapidly reversible and more slowly varying regulatory processes. Before describing the detailed mathematical structure of the model, we will highlight some general characteristics that the model must satisfy to capture the experimentally observed oscillatory quenching behavior of intact leaves. The model should:

1. Capture amplitude changes within periods without altering the empirically determined timescales.
2. Retain memory of previous cycles to describe slow envelopes of the maximum quenching and recovery.
3. Allow NPQ to turn on and off with rates that vary as a function of the illumination history.
4. Be agnostic about specific quenching mechanisms with all of the input parameters for the model determined directly from the experiment.
5. Be flexible enough to describe WT and all PsbS-containing mutants studied in this work.

The quenching giving rise to NPQ is thought to occur mainly within the light-harvesting complex proteins associated with PSII (LHCII),^{51,58,62–64} though LHCII is not necessarily the only site.^{63,65,66} Additionally, the quenching is likely the combined result of processes occurring on varying timescales, such as the relatively slow accumulation of Zea/Lut^{14,38,67,68} and/or membrane reorganization events^{69–71} as well as more rapid conformational changes within individual pigment–protein complexes.^{72–74} Therefore, our model treats slower regulatory processes as constraints on the result of the rapidly reversible regulation of quenching to incorporate the combined effects of the multiple timescales. Including interactions

between the various regulatory responses is a key difference from a model where the traditional quenching components (e.g., qE, qZ, and qI) arise from separate photochemical mechanisms and independent regulatory schemes.^{57,75} Our model is thus able to relate the multiple experimentally observed timescale responses to an overall extent of quenching (as opposed to biochemical observables) to draw conclusions about how the multiple regulatory responses combine to result in the overall quenching regulation on the seconds-to-minutes timescales.

A diagram of the regulatory model along with a table of the eight specific input parameters is shown in Scheme 1, and the detailed equations for the model are presented in Box 1. The model is based on the following differential equation

$$\frac{dq^{active}}{dt} = -[k_1(t) + k_2(t)]q^{active} + k_2(t)$$

which has a biexponential solution within each time period (the derivation is provided as an Appendix in the Supporting Information). q^{active} is the modeled variable that represents the trajectory of NPQ, and $k_1(t)$ and $k_2(t)$ are rate terms that describe the kinetics of turning NPQ off and on, respectively. These rates are piecewise defined to track whether the light is on or off at any given time during the experiment. Additionally, the rate terms are influenced by both the constant rates of induction or relaxation of the rapidly reversible quenching within a single period as well as the time-dependent state of the maximum quenching and maximum recovery envelopes. Therefore $k_1(t)$ and $k_2(t)$ (eqs 2 to 3) incorporate multi-timescale regulatory behavior through contributions from both rapid intraperiod processes ($k^{rapid}(t)$ terms as defined in eqs 4 to 5) and gradual interperiod processes ($k^{envelope}$ terms as defined in eqs 6–9).

Specifically, $k^{rapid}(t)$ contains the rapid intraperiod kinetics through τ_{ind}^{rapid} or τ_{rel}^{rapid} and the time-dependence arises from the slowly varying value of $q_{max}(t)$ or $q_{rec}(t)$ (eqs 4 and 5 in Box 1). Here, τ_{ind}^{rapid} and τ_{rel}^{rapid} are the constant best fit values of the time

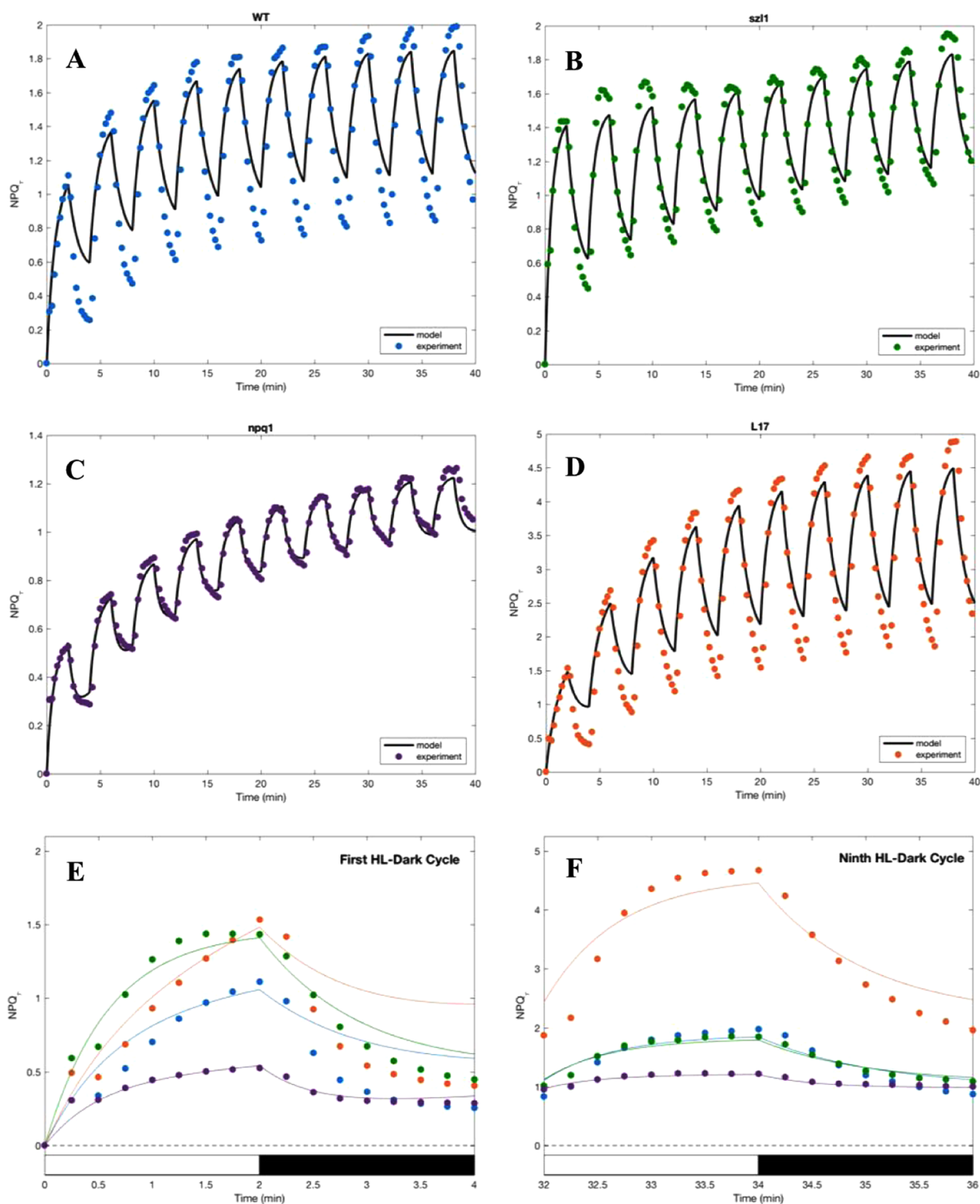


Figure 4. Comparison of model (solid lines) and experimental NPQ_τ values (closed circles) for all PsbS-containing lines: (A) WT (blue), (B) *szl1* (green), (C) *npq1* (purple), and (D) *L17* (orange). The first (E) and penultimate HL–dark cycles (F) are also shown for all strains. At the beginning of illumination (first HL–dark cycle), the model accurately captures the induction of quenching but does not fully capture the relaxation. The agreement is better for *npq1* that shows low magnitude oscillations as well as *szl1*, both of which lack *Zea*. By the end of the experiment (ninth HL–dark cycle), agreement between the model and experiment is improved, successfully capturing the induction and recovery dynamics. All model parameters are determined from best fit values of exponential decay fits of the maximum quenching and maximum recovery interperiod envelopes and the induction and relaxation of rapidly reversible intraperiod quenching reaching the quasi-periodic steady state. The simple model accurately depicts the nature of rapidly reversible quenching induction and relaxation occurring simultaneously with, and intertwined to, slower timescale quenching processes.

constants for the induction and relaxation of rapidly reversible quenching upon the envelopes reaching steady state in the final periods of the experimental data, as shown in Figure 3A,B and Table 3. $q_{\max}(t)$ and $q_{\text{rec}}(t)$ represent the time-dependent values of the maximum quenching and recovery envelope systems, respectively.

For both quenching and recovery, k^{envelope} is parametrized entirely based on τ_{\max}^{env} or $\tau_{\text{rec}}^{\text{env}}$, and c_{\max} or c_{rec} (eqs 6–9 in Box 1). τ_{\max}^{env} and $\tau_{\text{rec}}^{\text{env}}$ are the best fit time constants from exponential fits of the maximum quenching and recovery envelopes, respectively, obtained as previously described and shown in Figure 2A,B and Table 2. Similarly, c_{\max} and c_{rec} are the best fit additive constants, representing steady-state values of NPQ, obtained from the corresponding exponential fits of the envelopes. In our model construction, k^{envelope} is assumed to be constant on the timescale of the experiment, which is reasonable given that the state of the maximum quenching and maximum recovery envelopes varies slowly relative to the rapid induction or relaxation within periods.

It is important to note that both of the rate values $k_1(t)$ and $k_2(t)$ must change as a function of the HL–dark cycle number throughout the overall experimental time, instead of a simpler formulation where only a single rate value is modulated by the light or darkness. This is necessary to achieve a simultaneous agreement between the experimental data and the model (Figure S3). This is because the ratio of the rate constants (i.e., k_1/k_2) in the differential equation system determines the steady-state value (the maximum quenching or maximum recovery within a period). For a fixed recovery rate constant, either the induction rate or the resulting steady-state values can be accurately reproduced, but not both simultaneously.

With all the model parameters predetermined from direct fits of the data, the differential equation (eq 1 in Box 1) is solved numerically without subsequent fitting to obtain the model traces presented in Figure 4 for each mutant. The model satisfies the requirements previously mentioned, allowing it to describe the observed behavior of oscillatory quenching and recovery during HL and dark periods constrained by multiperiod envelopes with reasonable (but not perfect) accuracy. For example, while the model and experiment agree well for *sll1* (Figure 4B) and *npq1* (Figure 4C), the model's predicted NPQ dynamics deviate from the experimental values for WT (Figure 4A) and *L17* (Figure 4D), especially during early HL–dark cycles. Specifically, while the model successfully captures the induction of quenching during all HL periods (Table S1), the modeled traces for WT and *L17* do not capture the full relaxation of quenching during the early dark periods (Table S2). Yet the difference between the model and experiment, which is largest for the *L17* mutant at ~ 0.5 a unit of NPQ_τ (Figure 4D), still only corresponds to a relative error of 27% by the end of the ninth cycle, while most other strains have relative errors of 5% or less (Table S2). The difficulty of describing the *L17* trajectory using the model is not surprising given this mutant's larger dynamical range of oscillations in NPQ as a result of excess PsBs.

As alluded to earlier, perfect correspondence between the calculated and experimental values for NPQ_τ is not expected from a model that incorporates only minimal empirical kinetic data. As shown in Scheme 1, only eight empirical parameters are built into the structure of the model; six of these describe the interperiod maximum quenching and recovery envelopes and the remaining two represent the rates for intraperiod induction and relaxation. Therefore, the fidelity of the model in

describing the experiment relies on our ability to accurately extract these parameters from the exponential fits to the experimental data. In fact, by simply varying a single parameter, such as the intraperiod dark relaxation time constant $\tau_{\text{rel}}^{\text{rapid}}$, acceptable agreement between the model and experiment can be easily obtained for both WT and *L17* (Figure S4).

In general, the intraperiod induction of quenching is well reproduced during the early periods, while the intraperiod relaxation is not (Figure 4E; Tables S1 and S2). In contrast, during the later periods, both the induction and recovery are well described by our model (Figure 4F; Tables S1 and S2). We postpone for the discussion an analysis of these differences between the early and late periods of HL and darkness because we can draw important insights from them.

Despite the discrepancies between the model and experiment, the mathematical description allows the connection between the rapidly reversible regulation and the slower regulation to be highlighted: the model demonstrates how the initial induction of NPQ depends on both the induction timescale of rapidly reversible quenching and the slower timescale dynamics of the maximum quenching envelope. In other words, by accurately reproducing the changing magnitude of rapidly reversible quenching over successive HL–dark cycles, the model shows that the rapidly reversible regulation of quenching (qE) is likely intertwined with the status of the slower quenching processes (such as the qZ and qI components).

DISCUSSION

General Comments. Isolating quenching responses using periodic actinic light exposure reveals the complex, overlapping, and interdependent nature of the various regulatory processes contributing to observed nonphotochemical quenching in *A. thaliana*. For all strains, our data and analysis suggest that the traditional designation of the rapidly reversible component of NPQ, qE, cannot be described independently of the slower NPQ components, such as qZ or qI. The interdependence of fast and slow processes is in contrast to models in which each “timescale” component operates independently. This suggests that the components of quenching likely operate to regulate one or more common photochemical mechanism(s) in different ways, either through modification of the intrinsic quenching rate via rapidly inducible conformational changes within individual pigment–protein complexes or more slowly modulating the effective density of quenchers via chemical substitutions. Large-scale membrane organization changes are likely to further influence the connectivity of quenching sites to other areas of the photosynthetic antenna.

As stated in the methods, the plants are dark-adapted for 30 min before exposure to the periodic light sequence. Thus, during the first HL period both the fast and slow NPQ responses are initiated, which combine to generate the τ^{rapid} observed during the first several cycles. Interestingly, by the third cycle, the observed rapid intraperiod induction and relaxation kinetics have reached a steady state (Figure S2), while the slow processes continue to gradually approach full activation. Therefore, after the third cycle, the fast pathway becomes the dominant contributor to the intraperiod kinetics and consequently the observed values for τ^{rapid} appear unaffected by the illumination history.

The timescales of induction and relaxation within a single HL or dark period (Figures 3 and S2) and over the duration of

Table 4. Model Parameters and the Approximate Values for the Wild Type^a

	interperiod HL	interperiod dark	intraperiod HL	intraperiod dark
amplitude	$a_{\max} = -1$	$a_{\text{rec}} = -1$		
kinetics	$\tau_{\max}^{\text{env}} = 10 \text{ min}$	$\tau_{\text{rec}}^{\text{env}} = 10 \text{ min}$	$\tau_{\text{ind}}^{\text{rapid}} = 46 \text{ s}$	$\tau_{\text{rel}}^{\text{rapid}} = 85 \text{ s}$
steady state	$c_{\max} = 2$	$c_{\text{rec}} = 1$		

^aFor all of the exploratory calculations (presented in Figures 5 and S5), only one individual parameter is varied and the other seven are fixed to the experimental value for the wild type *A. thaliana*.

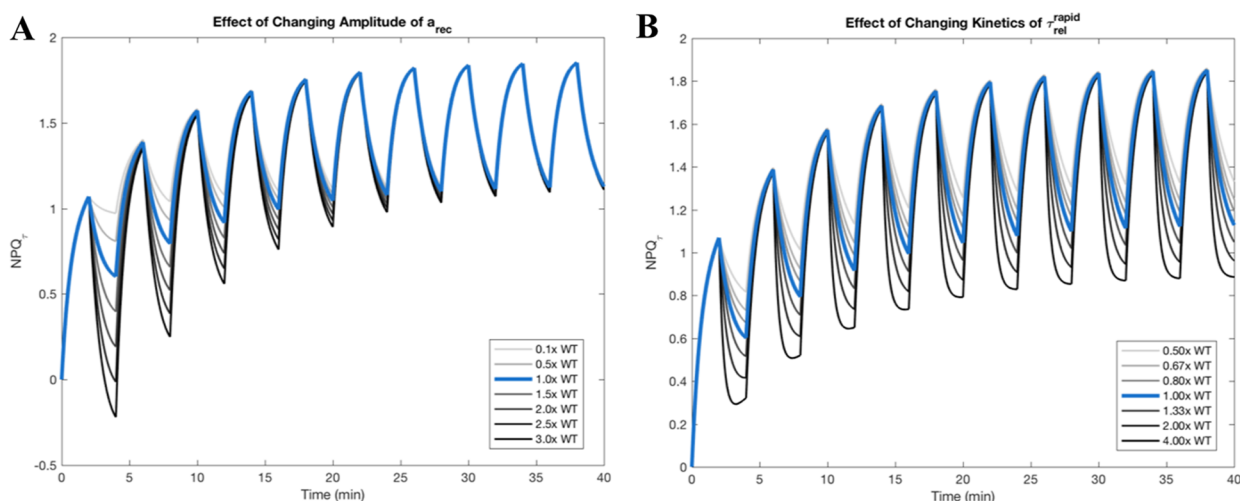


Figure 5. Predicted NPQ_r dynamics resulting from varying a single model parameter, while keeping the others fixed to the value of WT (listed in Table 4). (A) Influence of a_{\max} where the legend specifies the scaled amplitude relative to the wild type. For example, “2.0× WT” means $a_{\max} = 2 \times -1 = -2$. (B) Influence of $\tau_{\text{rel}}^{\text{rapid}}$ where the legend specifies the fractional improvement. For example, here, 2.00× WT signifies an acceleration of the kinetics by a factor of 2 relative to the wild type, or $\tau_{\text{rel}}^{\text{rapid}} = \frac{85}{2} = 43.5 \text{ s}$. For comparison, the model result when all eight parameters are set to the experimental value of WT is depicted by the thick blue line. For visual clarity, the white and black bars for the actinic light sequence have been omitted.

the 10 HL–dark cycles of our measurement (Figure 2) are quite similar for all of the mutants. An interesting exception is the *szl1* mutant that contains large quantities of Lut in the dark^{45,53} for which no exponential rise component is detectable for the maximum quenching envelope within the 15 s time resolution of these measurements. Instead, the maximum quenching envelope in *szl1* increased linearly, unlike all the other lines where the maximum NPQ_r envelope is well described by an exponential rise. This suggests that a relatively rapid conformational change in an individual pigment–protein complex is an initiator of quenching in *szl1*, rather than the slower or more complex membrane reorganization that may be necessary for the other strains. In contrast to the quenching envelope, the recovery envelope for *szl1* follows a similar mathematical form to the other lines, suggesting that *szl1* has a different “turn on” mechanism but a similar “turn off” mechanism compared to the other strains.

The plants reach steady state in quenching and recovery kinetics by cycle 3 (Figure S2). At steady state, the rapid intraperiod induction timescales are all similar at 30–50 s (Figure 3A and Table 3A). The recovery timescales are also similar to each other at 60–90 s (Figure 3B and Table 3B), though notably slower than induction. An exception is *npq1* which has a faster recovery time of $\sim 30 \text{ s}$, in agreement with reports in the literature.^{60,76}

Although our model was chosen to be agnostic about the underlying biochemical or photophysical mechanisms, by exploring the sensitivity of the modeled quenching magnitude and dynamics to the input model parameters, we are able to

make a number of conclusions from combining the data with the model. By fixing all the other parameters at their wild-type values (see Table 4), we explored how changes in a single parameter influence the overall response (Figures 5 and S5). For example, a_{\max} and a_{rec} , representing the amplitudes of the slowly evolving intraperiod envelopes $q_{\max}(t)$ and $q_{\text{rec}}(t)$, respectively, significantly influence the intraperiod behavior during the first few periods (see Figure S5A,B). In other words, the initial quenching response and the more gradual changes over multiple minutes should not be simply viewed as independent processes; the amplitude of the rapidly reversible component is intertwined with the state of the slower processes. For a model to reproduce this behavior it must retain this memory between periods since the biochemical systems do not fully relax to the dark-adapted state during the short, 2 min periods of darkness.

Next, we briefly discuss the insights on the roles of PsbS, the xanthophylls Zea and Lut, and ΔpH suggested by our data and model before making some final comments regarding potential uses of the model for improving biomass yields.

Role of PsbS. The role of PsbS in enabling the plant to respond to rapid changes in the light intensity is evident in *npq4* (lacks PsbS), which shows almost no modulation of quenching when cycling between HL and dark conditions (Figure 1). Surprisingly, the quenching response of *npq4* was observed to be “out-of-phase” with respect to the HL–dark periods (i.e., NPQ_r decreased during HL and increased during the dark). This finding, which will be discussed later in the context of the model, bolsters the idea that the pH-sensing

protein PsbS is necessary for the normal WT response to both HL and dark conditions.

When considering how PsbS interactions with LHCII might induce quenching, the simplest conceivable mechanism assumes that LHCII naturally favors an unquenched state, and when an interaction with protonated PsbS activated by ΔpH occurs, LHCII is forced into a quenched state.^{38,56,58,59,69,72,73,77} When ΔpH relaxes during the dark, the simplest assumption is that the interaction between PsbS and LHCII ceases, and LHCII can relax back to an unquenched state. This corresponds to a model description where only the induction rate (k_2) and not the relaxation rate (k_1) is modulated by the light and dark illumination sequence, but this is unable to reproduce the experimental results (Figure S3D–F). Therefore, the model suggests that not only do interactions between protonated PsbS and LHCII induce quenching, but that interactions between PsbS and LHCII might also actively induce recovery of LHCII from quenching, or at the very least that the protein interactions involved are not well described by such a simple kinetic scheme.

The role of PsbS in the relaxation of quenching is further supported by the exponential fits to the *L17* data, which give a larger value for a_{rec} (-2.33) than the wild type ($a_{\text{rec}} = -0.92$). All other mutants (disregarding *npq4*, which largely lacks an oscillatory quenching behavior) have a_{rec} values similar to the wild type. This comparison of *L17* and WT again raises the idea that PsbS may play a significant role in the rapid intraperiod relaxation of quenching during the dark. Assuming a WT structural and biochemical background, our model predicts that a value of $a_{\text{rec}} = -2.33$ would result in almost complete relaxation of NPQ during the first dark period (see the first dark period in Figure 5A), with decreasing percentages of full recovery as the steady-state response is reached.

In summary, a reasonable assumption may be that PsbS is involved in generating quenching sites leading to greater overall maximum NPQ values and less recovery (larger NPQ_τ values in the dark). However, we do not rule out that PsbS may also have more subtle or long-term effects, such as changing the membrane morphology or organization.^{56,58,59,70}

Roles of Zeaxanthin and Lutein. *npq1*, lacking *Zea*, shows substantially reduced modulation of quenching over HL–dark cycles compared to WT or *szl1* (though still greater than *npq4*) despite containing similar levels of PsbS. Unless there is excess Lut (as is the case for *szl1*), *Zea* is clearly required to obtain maximum quenching, though whether this implies a PsbS–*Zea* cooperativity or is simply additive is not clear. In the initial transition from the dark-adapted to HL conditions, very little violaxanthin to *Zea* conversion will occur.^{38,68,78} It therefore appears that at least the initial increase in NPQ_τ (the first few data points in each HL period) likely does not require *Zea*. However, *Zea* is clearly involved in slower quenching processes as the comparison of maximum quenching envelopes for WT and *szl1* shows, with WT beginning at smaller NPQ_τ max values and then reaching and slightly exceeding the value for *szl1* after three cycles (see Figure 2A). This gradual increase of NPQ_τ observed in WT could reflect the replacement of violaxanthin with *Zea* in LHCII in VDE enzyme-containing plants. *szl1* on the other hand, as noted above, lacks the exponential rise component in the maximum quenching envelope, suggesting that no pigment interchange and only a small conformational change is necessary to switch Lut into a quenching configuration in LHCII.

The picture of common photophysical mechanisms of energy dissipation controlled in different ways and with differing timescales of activation/deactivation could explain how *Zea* impacts multiple quenching processes: the substitution of *Zea* may influence an intrinsic rate of quenching or the density of quenching sites for which *Zea* plays a direct role, as well as influence structural properties of pigment–protein complexes that regulate conformational fluctuations and membrane organization that gradually activate additional or alternate quenching mechanisms.

Comparisons of Experimental and Modeled NPQ Trajectories. As mentioned above, by comparing the modeled NPQ_τ trajectory with the experimental data points, we are able to gain further insight into how the plant's most immediate response on exposure to HL or darkness depends on the illumination history. This analysis is centered around the fact that the model input for the intraperiod rapid responses comes only from the penultimate (ninth) periods; our model does not include any intraperiod input from the early illumination periods. Nonetheless, our empirically based kinetic model successfully captures the induction of quenching during all 10 HL–dark cycles (Figure 4 and Table S1). Thus, the steady-state intraperiod induction time constant ($\tau_{\text{ind}}^{\text{rapid}}$) seems sufficient to describe the plant's immediate response to HL and is independent of the illumination history. Since ΔpH is one of the fastest responses to HL exposure,^{13–15,57} this suggests that the kinetics of ΔpH formation may be unaffected by the illumination history.

On the other hand, our model is unable to reproduce the experimental dark relaxation dynamics during the early HL–dark cycles (Figure 4E and Table S2), but successfully captures the relaxation during the later dark periods (Figure 4F and Table S2). In other words, the rapid response associated with periodic exposure to darkness evolves (or changes) from cycle to cycle. Consequently, the steady-state relaxation time constant ($\tau_{\text{rel}}^{\text{rapid}}$) is a poor descriptor for the kinetics associated with quenching relaxation in the dark, especially during the early HL–dark cycles. Additionally, given that the agreement between the model and experiment during the early dark periods is better for the *Zea*-deficient *npq1* and *szl1* mutants, the cumulative rapid dark response seems to be dependent on *Zea*. In the future, time-resolved HPLC measurements⁷⁹ may provide additional insight into the roles of specific xanthophyll pigments during periodic illumination sequences. In vivo optical measurements of *Zea* formation^{60,80} and ΔpH ⁸¹ may provide additional clarity by allowing us to directly test the molecular basis for some of our observations.

Insights into NPQ Regulatory Processes. Returning to the structure of the model, we assume that $\tau_{\text{ind}}^{\text{rapid}}$ and $\tau_{\text{rel}}^{\text{rapid}}$ are constants modified by $q_{\text{max}}(t)$ or $q_{\text{rec}}(t)$ to give $k_1^{\text{rapid}}(t)$ and $k_2^{\text{rapid}}(t)$, respectively. This time independence of the rapid intraperiod dynamics is consistent with all of the mutant data after the first few cycles (Figure S2), i.e., when steady-state quenching and recovery are reached. At first glance, this might suggest that the rapid behavior does not depend on *Zea* or PsbS. However, the *Zea* concentration should be nearly constant by period 3 or 4 leading to similar rates of rapid NPQ relaxation. The *npq1* mutant shows a faster recovery, which is consistent with its lack of *Zea*. As we noted above, the interaction of PsbS with the antenna is likely more complex than a simple induction of quenching. If there are both short- and long-term influences of PsbS and, again, the long-term process(es) have reached a steady state by period 4, this could

explain the similarity of the quenching induction and recovery traces at the steady state (period 9; see Table 3 for timescales) when comparing the mutants (except for *npq4* that lacks both induction and recovery character).

Using our model we systematically explored the effects of omitting the slowly varying time-dependent state of the envelopes from the rapidly reversible rate constants (Figure S3). When $q_{\max}(t)$ is not included in $k^{\text{rapid}}(t)$, the model is unable to produce the expected response during HL or dark periods and, in fact, the response becomes out-of-phase (increasing NPQ_{τ} in the dark and decreasing NPQ_{τ} in HL) (Figure S3D,G). This out-of-phase behavior resembles the aforementioned experimental response for the *npq4* mutant under periodically fluctuating light (see red trace in Figure 1), further hinting that PsbS may play a role in both the HL and the dark response. Similar discrepancies between the model and experiment were also observed upon omitting $q_{\text{rec}}(t)$ from $k^{\text{rapid}}(t)$ (Figure S3E,H). Importantly, these findings reinforce the idea that the fast and slow processes involved in NPQ are inherently intertwined.

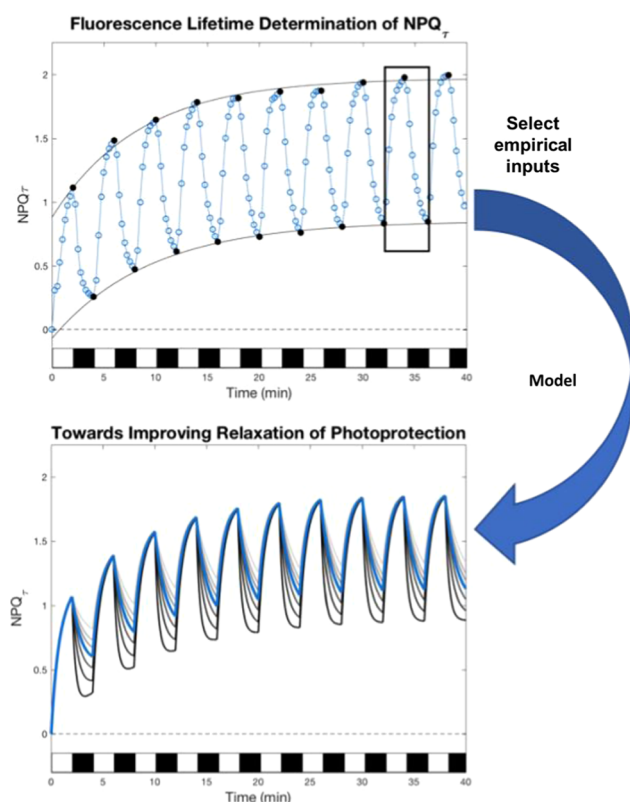
After fixing all of the model parameters at their wild-type values (see Table 4 and also the description in the SI), we also explored how changes in a single parameter influence the overall quenching response. Our exploration of the dependence of the eight parameters highlights the significance of two parameters— a_{rec} (the amplitude of the maximum recovery envelope) and $\tau_{\text{rel}}^{\text{rapid}}$ (the rate of intraperiod relaxation) (Figure 5; the effects of varying all 8 parameters are described in the SI and shown individually in Figure S5). Both quantities modulate the magnitude of NPQ relaxation without changing the extent of quenching. Therefore, optimizing these parameters could be an appropriate target for optimizing crop/biomass yields by accelerating the recovery from photoprotection while not compromising the plant's ability to protect itself under excess light. In future studies, periodic illumination will be a useful way to characterize new mutants with enhanced recovery amplitudes for improved biomass yields.

CONCLUDING REMARKS

A summary of the combined experimental and modeling approach employed in the present study is depicted in Scheme 2. Before discussing the implication of our analysis for efforts to optimize the NPQ response to enhance biomass yields, we briefly summarize the major findings from this work which, in some cases, differ significantly from conclusions based on single HL–dark measurement sequences.

- (1) The quenching response within individual periods as well as of the overall envelopes between periods lead to the conclusion that many timescales are very similar between the different mutants. The major effect of removing Zea or enhancing PsbS concentration is on the amplitudes of the slower (interperiod) induction and relaxation envelopes and not on their timescales. This is in contrast to conclusions from single HL–dark periods, which suggest that the qE component has the largest impact on quenching.
- (2) By comparing the model and experiment, it appears that the plant's immediate response to HL—aside from the initial transient response during the first two cycles—is independent of the illumination history, while the plant's immediate response to the dark evolves throughout

Scheme 2. Summary of the Approach Employed in This Study^a



^aFollowing the collection of fluorescence lifetime snapshot measurements on intact leaves under exposure to repeating cycles of 2 min HL and 2 min darkness, simple exponential fits were used to capture information about the interperiod (black data points and curves) and intraperiod dynamics (black box around cycle 9) for each mutant. Next, these empirical fit values were used as the sole inputs into the kinetic model, which is then able to describe the plant's overall response to repetitive HL and dark exposure with reasonable accuracy. Our model therefore provides a valuable framework to screen the ability of mutants to rapidly adjust NPQ to an illumination sequence that more closely resembles the fluctuating light conditions found in nature.

repeated HL–dark cycles and seems to be dependent on Zea.

- (3) Both PsbS and Zea/Lut have distinct roles in the NPQ response. For example, not only is PsbS required for the rapidly reversible quenching, but also longer timescale components likely involving changes in the membrane organization or morphology. In the absence of Zea, Lut can serve as an effective quencher, especially when present in increased amounts as is the case for the *szl1* mutant. Zea itself appears to be necessary for WT-levels of NPQ and is specifically involved in slower quenching processes.

As we have discussed previously, monitoring the quenching response throughout multiple light–dark cycles has the potential to reveal new insights into the complicated and overlapping nature of the various responses associated with NPQ induction and relaxation and the complex roles of the various molecular actors. The use of periodic illumination and the description of the data for five strains of *A. thaliana* clearly demonstrate that the rapidly reversible and slower responses to

excess light cannot be viewed independently. This interdependence of responses has important implications for efforts to optimize the NPQ response to increase yields in field growth conditions where plants are routinely subjected to fluctuating light.^{4,27}

Our analysis suggests that modifying the kinetics of the slow process does not appear to be a viable approach for increasing crop yields. Instead, by systematically varying the input parameters, our model suggests that attention should be focused on altering the amplitude of the slow recovery process (a_{rec}) as well as the kinetics of the rapidly reversible quenching process ($\tau_{\text{rel}}^{\text{rapid}}$; see **Box 1** and **Scheme 1** for definitions). Determining these parameters in the lab could provide a rapid method for selecting new mutants and overexpressors with enhanced recovery amplitudes for field trials aimed at increasing biomass yields.

Despite the potential for predictive power, kinetic models derived from fluorescence measurements alone cannot directly connect the understanding of dissipative mechanisms and structural processes from steady-state measurements to the observed regulation of fluorescence quenching dynamics. Snapshot transient absorption measurements have been developed that relate observables of quenching mechanisms to regulatory timescales.⁸² Further development of similar “snapshot” versions of techniques that can relate changes in protein conformation dynamics or membrane organization to these regulatory timescales will be necessary to integrate the understanding of physical phenomena with kinetic regulatory models. In addition, improved analysis methods for multi-period data sets such as those presented here should lead to more refined insights about the complicated and overlapping response of NPQ in the presence of dynamically changing light environments.

■ ASSOCIATED CONTENT

SI Supporting Information

The Supporting Information is available free of charge at <https://pubs.acs.org/doi/10.1021/acs.jpcb.0c06265>.

Analysis of fluorescence lifetime snapshot traces; description of model parameters; derivation of solution to model's differential equation (Appendix); snapshot fluorescence lifetime values collected from *A. thaliana* leaves (Figure S1); comparison of the intraperiod time constant as a function of the HL–dark cycle number (Figure S2); effect of removing the time-dependent slowly varying envelope components from the rapidly reversible rate constants in model eqs 4 and 5 (Figure S3); adjusting the intraperiod dark relaxation time constant (Figure S4); effect of varying each individual model parameter (Figure S5); comparison of the model and experiment after the first and penultimate high light periods (Table S1); and comparison of the model and experiment after the first and penultimate dark periods (Table S2) (PDF)

■ AUTHOR INFORMATION

Corresponding Author

Graham R. Fleming – Department of Chemistry, Graduate Group in Applied Science & Technology, and Graduate Group in Biophysics, University of California, Berkeley, California 94720, United States; Molecular Biophysics and Integrated Bioimaging Division, Lawrence Berkeley National

Laboratory, Berkeley, California 94720, United States; Kavli Energy Nanoscience Institute, Berkeley, California 94720, United States; orcid.org/0000-0003-0847-1838; Email: grfleming@lbl.gov

Authors

Collin J. Steen – Department of Chemistry, University of California, Berkeley, California 94720, United States; Molecular Biophysics and Integrated Bioimaging Division, Lawrence Berkeley National Laboratory, Berkeley, California 94720, United States; Kavli Energy Nanoscience Institute, Berkeley, California 94720, United States; orcid.org/0000-0002-7029-2892

Jonathan M. Morris – Molecular Biophysics and Integrated Bioimaging Division, Lawrence Berkeley National Laboratory, Berkeley, California 94720, United States; Kavli Energy Nanoscience Institute, Berkeley, California 94720, United States; Graduate Group in Applied Science & Technology, University of California, Berkeley, California 94720, United States

Audrey H. Short – Molecular Biophysics and Integrated Bioimaging Division, Lawrence Berkeley National Laboratory, Berkeley, California 94720, United States; Kavli Energy Nanoscience Institute, Berkeley, California 94720, United States; Graduate Group in Biophysics, University of California, Berkeley, California 94720, United States

Krishna K. Niyogi – Molecular Biophysics and Integrated Bioimaging Division, Lawrence Berkeley National Laboratory, Berkeley, California 94720, United States; Howard Hughes Medical Institute and Department of Plant and Microbial Biology, University of California, Berkeley, California 94720, United States

Complete contact information is available at:

<https://pubs.acs.org/10.1021/acs.jpcb.0c06265>

Author Contributions

C.J.S. and J.M.M. contributed equally to this work. J.M.M. and G.R.F. conceived the work; C.J.S. and J.M.M. designed the experiments; C.J.S., J.M.M., and A.H.S. performed the fluorescence measurements and analyzed the data; J.M.M. and C.J.S. developed and applied the model; C.J.S., J.M.M., and G.R.F. wrote the manuscript with input and comments from all authors.

Notes

The authors declare no competing financial interest.

The authors declare that all data supporting the findings of this study are available within the paper and its **Supporting Information** files.

The code utilized for the kinetic modeling in this study is available from the corresponding author G.R.F. upon request.

■ ACKNOWLEDGMENTS

The authors thank Cindy Amstutz and Masakazu Iwai for assistance with growing plants, Soomin Park for help troubleshooting the TCSPC laser apparatus, and Eric Arsenault, Paul Wrona, and Pallavi Bhattacharyya for valuable comments about the model and manuscript. We also thank the anonymous reviewers for multiple incisive comments that have improved the paper. This work was supported by the U.S. Department of Energy, Office of Science, Basic Energy Sciences, Chemical Sciences, Geosciences, and Biosciences Division under the field work proposal 449B. A.H.S. was

supported by the National Institutes of Health Molecular Biophysics Training Grant T32GM008295. K.K.N. is an investigator of the Howard Hughes Medical Institute.

REFERENCES

- (1) Blankenship, R. E. *Molecular Mechanisms of Photosynthesis*, 2nd ed.; Blackwell Science, 2014.
- (2) Demmig-Adams, B.; Garab, G.; Adams, W., III *Non-Photochemical Quenching and Energy Dissipation in Plants, Algae and Cyanobacteria*; Springer Netherlands, 2014.
- (3) Kromdijk, J.; Glowacka, K.; Leonelli, L.; Gabilly, S. T.; Iwai, M.; Niyogi, K. K.; Long, S. P. Improving Photosynthesis and Crop Productivity by Accelerating Recovery from Photoprotection. *Science* **2016**, *354*, 857–861.
- (4) Zhu, X.-G.; Ort, D. R.; Whitmarsh, J.; Long, S. P. The Slow Reversibility of Photosystem II Thermal Energy Dissipation on Transfer from High to Low Light May Cause Large Losses in Carbon Gain by Crop Canopies: A Theoretical Analysis. *J. Exp. Bot.* **2004**, *55*, 1167–1175.
- (5) Farooq, S.; Chmeliov, J.; Wientjes, E.; Koehorst, R.; Bader, A.; Valkunas, L.; Trinkunas, G.; van Amerongen, H. Dynamic Feedback of the Photosystem II Reaction Centre on Photoprotection in Plants. *Nat. Plants* **2018**, *4*, 225–231.
- (6) Melis, A. Photosystem-II Damage and Repair Cycle in Chloroplasts: What Modulates the Rate of Photodamage in Vivo? *Trends Plant Sci.* **1999**, *4*, 130–135.
- (7) Tyystjärvi, E.; Aro, E. M. The Rate Constant of Photoinhibition, Measured in Lincomycin-Treated Leaves, Is Directly Proportional to Light Intensity. *Proc. Natl. Acad. Sci. U.S.A.* **1996**, *93*, 2213–2218.
- (8) Keren, N.; Berg, A.; van Kan, P. J. M.; Levanon, H.; Ohad, I. Mechanism of Photosystem II Photoinactivation and D1 Protein Degradation at Low Light: The Role of Back Electron Flow. *Proc. Natl. Acad. Sci. U.S.A.* **1997**, *94*, 1579–1584.
- (9) Niyogi, K. K. Photoprotection Revisited: Genetic and Molecular Approaches. *Annu. Rev. Plant Physiol. Plant Mol. Biol.* **1999**, *50*, 333–359.
- (10) Demmig-Adams, B.; Adams, W. W. Photoprotection and Other Responses of Plants to High Light Stress. *Annu. Rev. Plant Physiol. Plant Mol. Biol.* **1992**, *43*, 599–626.
- (11) Ruban, A. V. Nonphotochemical Chlorophyll Fluorescence Quenching: Mechanism and Effectiveness in Protecting Plants from Photodamage. *Plant Physiol.* **2016**, *170*, 1903–1916.
- (12) Wraight, C. A.; Crofts, A. R. Energy-Dependent Quenching of Chlorophyll a Fluorescence in Isolated Chloroplasts. *Eur. J. Biochem.* **1970**, *17*, 319–327.
- (13) Briantais, J.-M.; Verrotte, C.; Picaud, M.; Krause, G. H. A Quantitative Study of the Slow Decline of Chlorophyll a Fluorescence in Isolated Chloroplasts. *Biochim. Biophys. Acta, Bioenerg.* **1979**, *548*, 128–138.
- (14) Noctor, G.; Rees, D.; Young, A.; Horton, P. The Relationship between Zeaxanthin, Energy-Dependent Quenching of Chlorophyll Fluorescence, and Trans-Thylakoid pH Gradient in Isolated Chloroplasts. *Biochim. Biophys. Acta, Bioenerg.* **1991**, *1057*, 320–330.
- (15) Goss, R.; Richter, M.; Wild, A. Role of ΔpH in the Mechanism of Zeaxanthin-Dependent Amplification of Q_E. *J. Photochem. Photobiol., B* **1995**, *27*, 147–152.
- (16) Müller, P.; Li, X.-P.; Niyogi, K. K. Non-Photochemical Quenching. A Response to Excess Light Energy. *Plant Physiol.* **2001**, *125*, 1558–1566.
- (17) de Bianchi, S.; Ballottari, M.; Dall'osto, L.; Bassi, R. Regulation of Plant Light Harvesting by Thermal Dissipation of Excess Energy. *Biochem. Soc. Trans.* **2010**, *38*, 651–660.
- (18) Dall'osto, L.; Caffarri, S.; Bassi, R. A Mechanism of Nonphotochemical Energy Dissipation, Independent from PsbS, Revealed by a Conformational Change in the Antenna Protein CP26. *Plant Cell* **2005**, *17*, 1217–1232.
- (19) Nilkens, M.; Kress, E.; Lambrev, P.; Miloslavina, Y.; Müller, M.; Holzwarth, A. R.; Jahns, P. Identification of a Slowly Inducible Zeaxanthin-Dependent Component of Non-Photochemical Quenching of Chlorophyll Fluorescence Generated under Steady-State Conditions in Arabidopsis. *Biochim. Biophys. Acta, Bioenerg.* **2010**, *1797*, 466–475.
- (20) Xu, P.; Tian, L.; Kloz, M.; Croce, R. Molecular Insights into Zeaxanthin-Dependent Quenching in Higher Plants. *Sci. Rep.* **2015**, *5*, No. 13679.
- (21) Tian, L.; Xu, P.; Chukhutsina, V. U.; Holzwarth, A. R.; Croce, R. Zeaxanthin-Dependent Nonphotochemical Quenching Does Not Occur in Photosystem I in the Higher Plant *Arabidopsis thaliana*. *Proc. Natl. Acad. Sci. U.S.A.* **2017**, *114*, 4828–4832.
- (22) Krause, G. H. Photoinhibition of Photosynthesis. An Evaluation of Damaging and Protective Mechanisms. *Physiol. Plant.* **1988**, *74*, 566–574.
- (23) Ruban, A. V.; Horton, P. An Investigation of the Sustained Component of Nonphotochemical Quenching of Chlorophyll Fluorescence in Isolated Chloroplasts and Leaves of Spinach. *Plant Physiol.* **1995**, *108*, 721–726.
- (24) Verhoeven, A. Sustained Energy Dissipation in Winter Evergreens. *New Phytol.* **2014**, *201*, 57–65.
- (25) Tian, Y.; Sacharz, J.; Ware, M. A.; Zhang, H.; Ruban, A. V. Effects of Periodic Photoinhibitory Light Exposure on Physiology and Productivity of Arabidopsis Plants Grown under Low Light. *J. Exp. Bot.* **2017**, *68*, 4249–4262.
- (26) Malnoë, A. Photoinhibition or Photoprotection of Photosynthesis? Update on the (Newly Termed) Sustained Quenching Component Q_H. *Environ. Exp. Bot.* **2018**, 123.
- (27) Külleim, C.; Ågren, J.; Jansson, S. Rapid Regulation of Light Harvesting and Plant Fitness in the Field. *Science* **2002**, *297*, 91–93.
- (28) Reinhardt, K.; Smith, W. K.; Carter, G. A. Clouds and Cloud Immersion Alter Photosynthetic Light Quality in a Temperate Mountain Cloud Forest. *Botany* **2010**, *88*, 462–470.
- (29) Slattery, R. A.; Walker, B. J.; Weber, A. P. M.; Ort, D. R. The Impacts of Fluctuating Light on Crop Performance. *Plant Physiol.* **2018**, *176*, 990–1003.
- (30) Kaiser, E.; Morales, A.; Harbinson, J. Fluctuating Light Takes Crop Photosynthesis on a Rollercoaster Ride. *Plant Physiol.* **2018**, *176*, 977–989.
- (31) Sylak-Glassman, E. J.; Zaks, J.; Amarnath, K.; Leuenberger, M.; Fleming, G. R. Characterizing Non-Photochemical Quenching in Leaves through Fluorescence Lifetime Snapshots. *Photosynth. Res.* **2016**, *127*, 69–76.
- (32) Baker, N. R. Chlorophyll Fluorescence: A Probe of Photosynthesis In Vivo. *Annu. Rev. Plant Biol.* **2008**, *59*, 89–113.
- (33) Kalaji, H. M.; Schansker, G.; Ladle, R. J.; Goltsev, V.; Bosa, K.; Allakhverdiev, S. I.; Brestic, M.; Bussotti, F.; Calatayud, A.; Dąbrowski, P.; et al. Frequently Asked Questions about in Vivo Chlorophyll Fluorescence: Practical Issues. *Photosynth. Res.* **2014**, *122*, 121–158.
- (34) Brugnoli, E.; Björkman, O. Chloroplast Movements in Leaves: Influence on Chlorophyll Fluorescence and Measurements of Light-Induced Absorbance Changes Related to ΔpH and Zeaxanthin Formation. *Photosynth. Res.* **1992**, *32*, 23–35.
- (35) Li, X.-P.; Björkman, O.; Shih, C.; Grossman, A. R.; Rosenquist, M.; Jansson, S.; Niyogi, K. K. A Pigment-Binding Protein Essential for Regulation of Photosynthetic Light Harvesting. *Nature* **2000**, *403*, 391–395.
- (36) Li, X.-P.; Gilmore, A. M.; Caffarri, S.; Bassi, R.; Golan, T.; Kramer, D. M.; Niyogi, K. K. Regulation of Photosynthetic Light Harvesting Involves Intrathylakoid Lumen pH Sensing by the PsbS Protein. *J. Biol. Chem.* **2004**, *279*, 22866–22874.
- (37) Li, X.-P.; Muller-Moule, P.; Gilmore, A. M.; Niyogi, K. K. PsbS-Dependent Enhancement of Feedback de-Excitation Protects Photosystem II from Photoinhibition. *Proc. Natl. Acad. Sci. U.S.A.* **2002**, *99*, 15222–15227.
- (38) Jahns, P.; Latowski, D.; Strzalka, K. Mechanism and Regulation of the Violaxanthin Cycle: The Role of Antenna Proteins and Membrane Lipids. *Biochim. Biophys. Acta, Bioenerg.* **2009**, *1787*, 3–14.

- (39) Ma, Y.-Z.; Holt, N. E.; Li, X.-P.; Niyogi, K. K.; Fleming, G. R. Evidence for Direct Carotenoid Involvement in the Regulation of Photosynthetic Light Harvesting. *Proc. Natl. Acad. Sci. U.S.A.* **2003**, *100*, 4377–4382.
- (40) Holt, N. E.; Zigmantas, D.; Valkūnas, L.; Li, X.-P.; Niyogi, K. K.; Fleming, G. R. Carotenoid Cation Formation and the Regulation of Photosynthetic Light Harvesting. *Science* **2005**, *307*, 433–436.
- (41) Bode, S.; Quentmeier, C. C.; Liao, P.-N.; Hafi, N.; Barros, T.; Wilk, L.; Bittner, F.; Walla, P. J. On the Regulation of Photosynthesis by Excitonic Interactions between Carotenoids and Chlorophylls. *Proc. Natl. Acad. Sci. U.S.A.* **2009**, *106*, 12311–12316.
- (42) Park, S.; Fischer, A. L.; Steen, C. J.; Iwai, M.; Morris, J. M.; Walla, P. J.; Niyogi, K. K.; Fleming, G. R. Chlorophyll-Carotenoid Excitation Energy Transfer in High-Light-Exposed Thylakoid Membranes Investigated by Snapshot Transient Absorption Spectroscopy. *J. Am. Chem. Soc.* **2018**, *140*, 11965–11973.
- (43) Park, S.; Steen, C. J.; Lyska, D.; Fischer, A. L.; Endelman, B.; Iwai, M.; Niyogi, K. K.; Fleming, G. R. Chlorophyll–Carotenoid Excitation Energy Transfer and Charge Transfer in Nannochloropsis Oceanica for the Regulation of Photosynthesis. *Proc. Natl. Acad. Sci. U.S.A.* **2019**, *116*, 3385–3390.
- (44) Ruban, A. V.; Berera, R.; Ilioaia, C.; van Stokkum, I. H. M.; Kennis, J. T. M.; Pascal, A. A.; van Amerongen, H.; Robert, B.; Horton, P.; van Grondelle, R. Identification of a Mechanism of Photoprotective Energy Dissipation in Higher Plants. *Nature* **2007**, *450*, 575–578.
- (45) Li, Z.; Ahn, T. K.; Avenson, T. J.; Ballottari, M.; Cruz, J. A.; Kramer, D. M.; Bassi, R.; Fleming, G. R.; Keasling, J. D.; Niyogi, K. K. Lutein Accumulation in the Absence of Zeaxanthin Restores Nonphotochemical Quenching in the *Arabidopsis thaliana* Npq1 Mutant. *Plant Cell* **2009**, *21*, 1798–1812.
- (46) Mascoli, V.; Liguori, N.; Xu, P.; Roy, L. M.; van Stokkum, I. H. M.; Croce, R. Capturing the Quenching Mechanism of Light-Harvesting Complexes of Plants by Zooming in on the Ensemble. *Chem* **2019**, 2900.
- (47) Cupellini, L.; Calvani, D.; Jacquemin, D.; Mennucci, B. Charge Transfer from the Carotenoid Can Quench Chlorophyll Excitation in Antenna Complexes of Plants. *Nat. Commun.* **2020**, *11*, No. 662.
- (48) Niyogi, K. K.; Grossman, A. R.; Björkman, O. Arabidopsis Mutants Define a Central Role for the Xanthophyll Cycle in the Regulation of Photosynthetic Energy Conversion. *Plant Cell* **1998**, *10*, 1121–1134.
- (49) Havaux, M.; Niyogi, K. K. The Violaxanthin Cycle Protects Plants from Photooxidative Damage by More than One Mechanism. *Proc. Natl. Acad. Sci. U.S.A.* **1999**, *96*, 8762–8767.
- (50) Cazzaniga, S.; Li, Z.; Niyogi, K. K.; Bassi, R.; Dall’Osto, L. The Arabidopsis Szl1 Mutant Reveals a Critical Role of β -Carotene in Photosystem I Photoprotection. *Plant Physiol.* **2012**, *159*, 1745–1758.
- (51) Schansker, G.; Tóth, S. Z.; Strasser, R. J. Dark Recovery of the Chl *a* Fluorescence Transient (OJIP) after Light Adaptation: The QT-Component of Non-Photochemical Quenching Is Related to an Activated Photosystem I Acceptor Side. *Biochim. Biophys. Acta, Bioenerg.* **2006**, *1757*, 787–797.
- (52) Sylak-Glassman, E. J.; Malnoë, A.; De Re, E.; Brooks, M. D.; Fischer, A. L.; Niyogi, K. K.; Fleming, G. R. Distinct Roles of the Photosystem II Protein PsbS and Zeaxanthin in the Regulation of Light Harvesting in Plants Revealed by Fluorescence Lifetime Snapshots. *Proc. Natl. Acad. Sci. U.S.A.* **2014**, *111*, 17498–17503.
- (53) Leuenberger, M.; Morris, J. M.; Chan, A. M.; Leonelli, L.; Niyogi, K. K.; Fleming, G. R. Dissecting and Modeling Zeaxanthin- and Lutein-Dependent Nonphotochemical Quenching in *Arabidopsis thaliana*. *Proc. Natl. Acad. Sci. U.S.A.* **2017**, *114*, E7009–E7017.
- (54) Bennett, D. I. G.; Amarnath, K.; Park, S.; Steen, C. J.; Morris, J. M.; Fleming, G. R. Models and Mechanisms of the Rapidly Reversible Regulation of Photosynthetic Light Harvesting. *Open Biol.* **2019**, *9*, No. 190043.
- (55) Park, S.; Fischer, A. L.; Li, Z.; Bassi, R.; Niyogi, K. K.; Fleming, G. R. Snapshot Transient Absorption Spectroscopy of Carotenoid Radical Cations in High-Light-Acclimating Thylakoid Membranes. *J. Phys. Chem. Lett.* **2017**, *8*, 5548–5554.
- (56) Johnson, M. P.; Ruban, A. V. Arabidopsis Plants Lacking PsbS Protein Possess Photoprotective Energy Dissipation. *Plant J.* **2010**, *61*, 283–289.
- (57) Zaks, J.; Amarnath, K.; Kramer, D. M.; Niyogi, K. K.; Fleming, G. R. A Kinetic Model of Rapidly Reversible Nonphotochemical Quenching. *Proc. Natl. Acad. Sci. U.S.A.* **2012**, *109*, 15757–15762.
- (58) Correa-Galvis, V.; Poschmann, G.; Melzer, M.; Stühler, K.; Jahns, P. PsbS Interactions Involved in the Activation of Energy Dissipation in Arabidopsis. *Nat. Plants* **2016**, *2*, No. 15225.
- (59) Sacharz, J.; Giovagnetti, V.; Ungerer, P.; Mastroianni, G.; Ruban, A. V. The Xanthophyll Cycle Affects Reversible Interactions between PsbS and Light-Harvesting Complex II to Control Non-Photochemical Quenching. *Nat. Plants* **2017**, *3*, No. 16225.
- (60) Johnson, M. P.; Pérez-Bueno, M. L.; Zia, A.; Horton, P.; Ruban, A. V. The Zeaxanthin-Independent and Zeaxanthin-Dependent QE Components of Nonphotochemical Quenching Involve Common Conformational Changes within the Photosystem II Antenna in Arabidopsis. *Plant Physiol.* **2009**, *149*, 1061–1075.
- (61) Roach, T.; Krieger-Liszka, A. The Role of the PsbS Protein in the Protection of Photosystems I and II against High Light in *Arabidopsis thaliana*. *Biochim. Biophys. Acta, Bioenerg.* **2012**, *1817*, 2158–2165.
- (62) Townsend, A. J.; Saccon, F.; Giovagnetti, V.; Wilson, S.; Ungerer, P.; Ruban, A. V. The Causes of Altered Chlorophyll Fluorescence Quenching Induction in the Arabidopsis Mutant Lacking All Minor Antenna Complexes. *Biochim. Biophys. Acta, Bioenerg.* **2018**, *1859*, 666–675.
- (63) Nicol, L.; Nawrocki, W. J.; Croce, R. Disentangling the Sites of Non-Photochemical Quenching in Vascular Plants. *Nat. Plants* **2019**, *5*, 1177–1183.
- (64) Saccon, F.; Giovagnetti, V.; Shukla, M. K.; Ruban, A. V. Rapid Regulation of Photosynthetic Light Harvesting in the Absence of Minor Antenna and Reaction Centre Complexes. *J. Exp. Bot.* **2020**, 3626.
- (65) Dall’Osto, L.; Cazzaniga, S.; Bressan, M.; Paleček, D.; Židek, K.; Niyogi, K. K.; Fleming, G. R.; Zigmantas, D.; Bassi, R. Two Mechanisms for Dissipation of Excess Light in Monomeric and Trimeric Light-Harvesting Complexes. *Nat. Plants* **2017**, *3*, No. 17033.
- (66) Ruban, A. V.; Johnson, M. P.; Duffy, C. D. P. The Photoprotective Molecular Switch in the Photosystem II Antenna. *Biochim. Biophys. Acta, Bioenerg.* **2012**, *1817*, 167–181.
- (67) Demmig, B.; Winter, K.; Krüger, A.; Czygan, F. C. Photoinhibition and Zeaxanthin Formation in Intact Leaves: A Possible Role of the Xanthophyll Cycle in the Dissipation of Excess Light Energy. *Plant Physiol.* **1987**, *84*, 218–224.
- (68) Gilmore, A. M.; Mohanty, N.; Yamamoto, H. Y. Epoxidation of Zeaxanthin and Antheraxanthin Reverses Non-Photochemical Quenching of Photosystem II Chlorophyll *a* Fluorescence in the Presence of Trans-Thylakoid Δ pH. *FEBS Lett.* **1994**, *350*, 271–274.
- (69) Goral, T. K.; Johnson, M. P.; Duffy, C. D. P.; Brain, A. P. R.; Ruban, A. V.; Mullineaux, C. W. Light-Harvesting Antenna Composition Controls the Macrostructure and Dynamics of Thylakoid Membranes in Arabidopsis. *Plant J.* **2012**, *69*, 289–301.
- (70) Albanese, P.; Tamara, S.; Saracco, G.; Scheltema, R. A.; Pagliano, C. How Paired PSII–LHCII Supercomplexes Mediate the Stacking of Plant Thylakoid Membranes Unveiled by Structural Mass-Spectrometry. *Nat. Commun.* **2020**, *11*, No. 1361.
- (71) Anderson, J. M.; Horton, P.; Kim, E.-H.; Chow, W. S. Towards Elucidation of Dynamic Structural Changes of Plant Thylakoid Architecture. *Philos. Trans. R. Soc., B* **2012**, *367*, 3515–3524.
- (72) Johnson, M. P.; Goral, T. K.; Duffy, C. D. P.; Brain, A. P. R.; Mullineaux, C. W.; Ruban, A. V. Photoprotective Energy Dissipation Involves the Reorganization of Photosystem II Light-Harvesting Complexes in the Grana Membranes of Spinach Chloroplasts. *Plant Cell* **2011**, *23*, 1468–1479.

(73) Kiss, A. Z.; Ruban, A. V.; Horton, P. The PsbS Protein Controls the Organization of the Photosystem II Antenna in Higher Plant Thylakoid Membranes. *J. Biol. Chem.* **2008**, *283*, 3972–3978.

(74) Betterle, N.; Ballottari, M.; Zorzan, S.; de Bianchi, S.; Cazzaniga, S.; Dall'osto, L.; Morosinotto, T.; Bassi, R. Light-Induced Dissociation of an Antenna Hetero-Oligomer Is Needed for Non-Photochemical Quenching Induction. *J. Biol. Chem.* **2009**, *284*, 15255–15266.

(75) Morris, J. M.; Fleming, G. R. Quantitative Modeling of Energy Dissipation in *Arabidopsis thaliana*. *Environ. Exp. Bot.* **2018**, *99*.

(76) Zia, A.; Johnson, M. P.; Ruban, A. V. Acclimation- and Mutation-Induced Enhancement of PsbS Levels Affects the Kinetics of Non-Photochemical Quenching in *Arabidopsis thaliana*. *Planta* **2011**, *233*, 1253–1264.

(77) Ware, M. A.; Giovagnetti, V.; Belgio, E.; Ruban, A. V. PsbS Protein Modulates Non-Photochemical Chlorophyll Fluorescence Quenching in Membranes Depleted of Photosystems. *J. Photochem. Photobiol., B* **2015**, *152*, 301–307.

(78) Matuszyńska, A.; Heidari, S.; Jahns, P.; Ebenhöf, O. A Mathematical Model of Non-Photochemical Quenching to Study Short-Term Light Memory in Plants. *Biochim. Biophys. Acta, Bioenerg.* **2016**, *1857*, 1860–1869.

(79) Müller-Moulé, P.; Conklin, P. L.; Niyogi, K. K. Ascorbate Deficiency Can Limit Violaxanthin De-Epoxidase Activity in Vivo. *Plant Physiol.* **2002**, *128*, 970–977.

(80) Zhang, R.; Kramer, D. M.; Cruz, J. A.; Struck, K. R.; Sharkey, T. D. The Effects of Moderately High Temperature on Zeaxanthin Accumulation and Decay. *Photosynth. Res.* **2011**, *108*, 171–181.

(81) Takizawa, K.; Cruz, J. A.; Kanazawa, A.; Kramer, D. M. The Thylakoid Proton Motive Force in Vivo. Quantitative, Non-Invasive Probes, Energetics, and Regulatory Consequences of Light-Induced Pmf. *Biochim. Biophys. Acta, Bioenerg.* **2007**, *1767*, 1233–1244.

(82) Park, S.; Steen, C. J.; Fischer, A. L.; Fleming, G. R. Snapshot Transient Absorption Spectroscopy: Toward in Vivo Investigations of Nonphotochemical Quenching Mechanisms. *Photosynth. Res.* **2019**, *141*, 367–376.